1521-0103/382/2/113–122$35.00
THE JOURNAL OF PHARMACOLOGY AND EXPERIMENTAL THERAPEUTICS

dx.doi.org/10.1124/jpet.122.001248
J Pharmacol Exp Ther 382:113–122, August 2022

The Journal of PHARMACOLOGY And Experimental Therapeutics

Nafamostat is a Potent Human Diamine Oxidase Inhibitor Possibly Augmenting Hypersensitivity Reactions during Nafamostat Administration

Thomas Boehm, Marion Alix, Karin Petroczi, Serhii Vakal, Elisabeth Gludovacz, Nicole Borth, Tiina A. Salminen, and Bernd Jilma

Department of Clinical Pharmacology, Medical University of Vienna, Vienna, Austria (T.B., K.P., E.G., B.J.); Structural Bioinformatics Laboratory, Biochemistry, Faculty of Science and Engineering (M.A., S.V., T.A.S.), and InFLAMES Research Flagship Center (M.A., S.V., T.A.S.), Åbo Akademi University, Turku, Finland; and Department of Biotechnology, University of Natural Resources and Life Sciences, Vienna, Austria (E.G., N.B.)

Received April 1, 2022; accepted May 16, 2022

ABSTRACT

Nafamostat is an approved short-acting serine protease inhibitor. However, its administration is also associated with anaphylactic reactions. One mechanism to augment hypersensitivity reactions could be inhibition of diamine oxidase (DAO). The chemical structure of nafamostat is related to the potent DAO inhibitors pentamidine and diminazene. Therefore, we tested whether nafamostat is a human DAO inhibitor. Using different activity assays, nafamostat reversibly inhibited recombinant human DAO with an IC_{50} of 300–400 nM using 200 μM substrate concentrations. The K_i of nafamostat for the inhibition of putrescine and histamine deamination is 27 nM and 138 nM, respectively For both substrates, nafamostat is a mixed mode inhibitor with *P* values of <0.01 compared with other inhibition types. Using 80–90% EDTA plasma, the IC_{50} of nafamostat inhibition was approximately 360 nM using 20 μM cadaverine. In 90% EDTA plasma, the IC_{50} concentrations were 2–3 μM using 0.9 μM and 0.18 μM histamine as substrate. In silico modeling showed a high overlap compared with published diminazene crystallography data, with a preferred orientation of the guanidine group toward topaquinone. In conclusion, nafamostat is a potent human DAO inhibitor and might increase severity of anaphylactic reaction by interfering with DAO-mediated extracellular histamine degradation.

SIGNIFICANCE STATEMENT

Treatment with the short-acting anticoagulant nafamostat during hemodialysis, leukocytapheresis, extracorporeal membrane oxygenator procedures, and disseminated intravascular coagulation is associated with severe anaphylaxis in humans. Histamine is a central mediator in anaphylaxis. Potent inhibition of the only extracellularly histamine-degrading enzyme diamine oxidase could augment anaphylaxis reactions during nafamostat treatment.

Introduction

Nafamostat [(6-carbamimidoylnaphthalen-2-yl) 4-(diaminomethylideneamino)benzoate; Futhan; Fut-175] is a serine-protease inhibitor of various enzymes such as thrombin, factor Xa, factor XIIa, plasmin, or kallikrein (Aoyama et al., 1984; Fujii and Hitomi, 1981; Hitomi et al., 1985; Okajima et al., 1995). For several decades, it has been used as a treatment of pancreatitis and also as a short-acting anticoagulant for hemodialysis, leukocytapheresis, extracorporeal membrane oxygenator (ECMO) procedures, and disseminated intravascular coagulation (Han et al., 2011; Sawada et al., 2016; Minakata et al., 2019). Nafamostat is additionally considered a new treatment option for coronavirus disease (COVID-19), because it inhibits transmembrane protease serine 2 (TMPSS2), which is involved in severe acute respiratory syndrome coronavirus 2 (SARS-CoV-2) entry into target cells (Hoffmann et al., 2020; Asakura and Ogawa, 2020; Hempel et al., 2021; Yamamoto et al., 2020).

At a steady infusion rate of 0.2 mg/kg/h, nafamostat plasma concentrations reached 90 and 240 nM (Mori et al., 2003). For nafamostat treatment during ECMO, a mean dosage of 0.64 mg/kg/h was used. This would correspond to concentrations between 288 and 768 nM (Han et al., 2011). Some patients received 1.15–2.19 mg/kg/h, resulting in plasma concentrations between 518 and 2628 nM. During cardiopulmonary bypass (CPB), 0.2 mg/kg/h nafamostat was administered before and after CPB and 2 mg/kg/h during CBP (Miyamoto et al., 1992; Sakamoto et al., 2014). These high-dose infusion rates result in μM nafamostat plasma concentrations. The volume of distribution of nafamostat calculated using five healthy volunteers was 0.36 L/kg or 25.2 L in a person with 70 kg bodyweight but only 0.08 L/kg in 8 hemodialysis patients (Osono et al., 1991). The lower

This work was supported by the InFLAMES Flagship Program of the Academy of Finland [decision number: 337530] and the Sigrid Juselius foundation.
dx.doi.org/10.1124/jpet.122.001248.
This article has supplemental material available at jpet.aspetjournals.org.

ABBREVIATIONS: DAO, diamine oxidase; H_2O_2, hydrogen peroxide; HRP, horseradish peroxidase; HSA, human serum albumin; K_i, inhibitory constant.

volume of distribution in hemodialysis patients was attributed to a possible arterialvenous fistula (Osono et al., 1991).

Camostat (4-[2-[2-(dimethylamino)-2-oxoethoxy]-2-oxoethyl]-phenyl] 4-(diaminomethylideneamino)benzoate; Foipan) is a related serine-protease inhibitor used for the treatment of chronic pancreatitis and postoperative reflux esophagitis. No cases of anaphylaxis have been associated with camostat, but this may be because it is used much less frequently compared with nafamostat, and also because it is not used during extracorporeal circulation treatment. Camostat is only a precursor and is rapidly degraded in the liver to the active 4-(4-guanidinobenzoyloxy)phenylacetic acid (Midgley et al., 1994).

Several reports of nafamostat-induced anaphylactic reactions have been published in patients undergoing hemodiafiltration (Maruyama et al., 1996; Ookawara et al., 2018; Kim et al., 2016; Kim et al., 2021). When compared with that demonstrated by heparin, the adverse reaction profile during leukocytapheresis showed increased rates of "typical" histamine-mediated symptoms such as headache, nausea, rash, itching, palpitations, dyspnea, and anaphylactic shock (Sawada et al., 2016). Miyamoto et al. (1992) measured increased histamine concentrations during CBP using high dose nafamostat and suggested that nafamostat might be a diamine oxidase (DAO) inhibitor.

Human DAO (E.C. 1.4.3.22) is a copper-containing amine oxidase that oxidatively deaminates histamine and various polyamines, releasing ammonia and hydrogen peroxide (Elmore et al., 2002). In humans, high DAO mRNA levels and enzymatic activity were measured in the gastrointestinal tract with increased concentrations in the duodenum and ileum/jejunum compared with the colon. In addition, high levels were found in the proximal tubular epithelial cells of the kidneys and in the extravillous trophoblast cells, fetal cells invading the decidua and the myometrium during placenta development (Elmore et al., 2002; Schwelberger et al., 1998a; Schwelberger et al., 1998a; Velicky et al., 2018). Plasma DAO concentrations increase at least 100-fold during pregnancy (Southren et al., 1964; Boehm et al., 2017). In two large animal studies involving pigs and sheep, irreversible pharmacological inhibition of DAO activity using high doses of aminoguanidine resulted in increased morbidity and mortality after exogenous histamine challenge (Sattler et al., 1988; Sjaastad, 1967). Nevertheless, the role of DAO in the elimination of endogenous histamine during anaphylaxis or during mast cell activation is not clear.

The symmetrical diamidines, pentamidine and diminazene, are potent DAO inhibitors (McGrath et al., 2009; Duch et al., 1984). Although nafamostat is not a classic diamidine and is not symmetrical, it could be a potent DAO inhibitor because it contains one terminal amidinium and one terminal guanidinium moiety, in addition to a naphthyl group. Two of the most potent DAO inhibitors, isometamidium and prothidium, contain a phenanthridine triple aromatic ring structure and two additional individual aromatic rings (Duch et al., 1984). The marginally less active antricyde is composed of a quinoline group, a double aromatic ring like naphthalene, and a benzyl ring (Duch et al., 1984). For efficient DAO inhibition, aromatic ring structures in combination with terminal amidinium/guanidinium moieties and several nitrogen atoms are clearly important. Amiloride contains seven nitrogen atoms and a pyrazine aromatic ring but is a much weaker DAO inhibitor compared with phenamil or benzamil, which carry a second aromatic ring, phenyl or benzyl group, respectively, linked to the guanidinium moiety of amiloride (Novotny et al., 1994).

If DAO is potently inhibited by nafamostat, endogenous histamine degradation might be impaired during nafamostat administration, possibly augmenting hypersensitivity reactions. In a first step toward answering this clinically relevant question, we tested whether nafamostat is a bona fide human DAO inhibitor.

Materials and Methods

References used only in the Material and Methods section are listed in the Supplemental Material. In this section only numbers are assigned. If the reference is also used in other sections, it is regularly listed with name and year.

Chemicals and reagents. Albunorm (Octapharma, Vienna, Austria), a 20% human serum albumin (HSA) solution, is authorized for human use and 96% of the protein content is HSA. Its other ingredients, 16.8 mM caprylic acid and 16.8 mM N-acetyl-tryptophan, do not inhibit DAO activity. PBS pH 7.4 without $MgCl_2$ and $CaCl_2$ was purchased from Gibco (Vienna, Austria). Diminazene aceturate (D7770), DMSO (D2650), putrescine (P5780), cadaverine (C8561), histamine (53300), ortho-aminobenzaldehyde (A9628), horse radish peroxidase (HRP; P6782), amiloride (A7410), benzamil (B2417), phenamil (P203), camostat (SML0057), sodium fluoride (201154), phenylhydrazine (114715), methylhydrazine (M50001), 2-hydroxyquinoline (270873), glucose oxidase (G6125), ethyl acetate (34858), DNTB (Ellman's reagent; D8130), vanillic acid (94770), and 4-aminoantipyrine (33528) were purchased from Sigma-Aldrich (Vienna, Austria). Nafamostat was purchased from Torii Pharmaceuticals (Futhan) and Cayman (14837; Vienna, Austria). Aminoguanidine (81530) was bought from Cayman. Foipan tablets and 5% glucose solution were provided by the pharmacy at the General Hospital Vienna. Naphthalene-2-yl-benzoate (330610050) and Amplex red (12222) were purchased from Thermo Fisher Scientific (Vienna, Austria). If not otherwise indicated, compounds were dissolved in DMSO at 10 mM and stored at −32°C for no longer than 2 years or were freshly prepared and used immediately. Foipan tablets were ground and dissolved in DMSO or water at a 10 mM camostat concentration. The DMSO solution was clear and used immediately. The water solution was centrifuged at high speed for 5 minutes, and the supernatant was assumed to contain 10 mM camostat.

DAO Activity Assay Using Hydrogen Peroxide HRP Coupling with Luminol, Amplex Red or Vanillic Acid/4-Aminoantipyrine. The luminol DAO activity assay is based on a published luminescence assay (Supplemental Ref. 1) and is described in detail (Boehm et al., 2020). The expression and purification of recombinant human DAO in Chinese hamster ovary cells has been previously published (Supplemental Ref. 2). Final DAO concentrations were 0.2–1 μg/ml (1.2–6 nM based on the dimer and excluding the molecular weight of the extensive glycosylation), quantified using absorption measurements or using an in-house developed DAO ELISA (Boehm et al., 2017). For activity assays we used 0.05–0.1% HSA PBS buffer or 80–90% plasma from healthy volunteers as matrix. The pH of the luminol solution from a commercial ECL Western blotting kit (Amersham RPN2106; Vienna, Austria) was adjusted from 9.2 to 8.0. The lower pH is closer to a physiologically relevant pH level, and the quantum yield is still sufficiently high to effectively measure DAO activity.

Using 50 μM Amplex red instead of luminol allows H_2O_2–HRP coupling in HSA PBS buffer with higher sensitivity. It also allows for easier oxidation rate calculations because the assay can be performed using continuous measurements with accumulating stable resorufin (Boehm et al., 2020).

We also used H_2O_2–HRP vanillic acid/4-aminoantipyrine coupling as described (Supplemental Ref. 3). The chromophore measured at 490 nm is relatively pH insensitive between pH 6 and pH 10. This

assay was also used to measure the potency of nafamostat between pH 6 and 10 using the Britton-Robinson buffer system with 0.1% HSA (Supplemental Ref. 4).

DAO Activity Assay Using P-Dimethylaminomethylbenzylamine Oxidation. The presence of antioxidants or other molecules interfering with H_2O_2-HRP coupling distort proper DAO activity measurements (Boehm et al., 2020). Dimethylaminomethylbenzylamine is a substrate for DAO, which can be directly quantified. However, the Michaelis constant (Km) is only 110 μM or approximately 5.5- to 39-fold higher than putrescine and histamine, respectively (Elmore et al., 2002; Boehm et al., 2020). We used a benzaldehyde extinction coefficient of 11000 $M^{-1}cm^{-1}$ at 250 nm for rate calculations. This value is about 100-fold higher than the benzylamine moiety of the parent compound. UV-compatible 96-well half-area plates (UltraCruz UV plates; SCBT; Heidelberg, Germany) were used. An HSA concentration of 0.05% reduced the protein-based signal at 250 nm to acceptable levels.

DAO Activity Assay Using Fluorescence Measurements. DAO generates δ-1-piperideine (2,3,4,5-tetrahydro-pyridine), the autocyclized reaction product, using cadaverine as substrate. The condensate between δ-1-piperideine and ortho-aminobenzaldehyde (oABA; stored at −32°C for 4 to 6 months as a 200 mM stock solution in absolute ethanol) generates 5,5a,6,7,8,9-hexahydropyrido[2,1-[b]]quinazoline-10-ium or abbreviated HHPQ. Absorption and fluorescence measurement procedures of HHPQ using a Synergy H1 Multi-Mode Microplate reader (BioTek; Winooski, Vermont) have been published (Boehm et al., 2020).

For the detection of HHPQ in plasma from healthy volunteers, we mixed 85 μl plasma adjusted to pH 7.4 with 11 μl 1 M HCl per ml of plasma with 5 μl 10% ethanol or 5 μl 20 mM oABA and 5 μl PBS or 5 μl 4 mM cadaverine and 5 μl 20-fold concentrated inhibitors. Only 80 μl plasma was used testing in addition the influence of esterase inhibitors. All samples were analyzed in duplicate. After incubation for 30 minutes to 1 hour at 37°C in the dark, 200 μl 7.5% TCA (99.5% trichloroacetic acid; 91228; Sigma-Aldrich; Vienna, Austria) was added and the solution incubated on ice for 20 minutes. After 10 minutes of high speed centrifugation, 150–200 μl were recovered and fluorescence was measured as described (Boehm et al., 2020).

Measurement of Histamine Concentrations. Histamine concentrations were measured using the homogeneous time-resolved fluorescence histamine dynamic kit (62HTMPEG) from Cisbio (now Perkin Elmer) according to the instructions. However, the concentration range was adjusted to the spiked histamine concentrations. In addition, a standard curve using in-house histamine was used, rather than the histamine provided in the kit. Dilutions were selected to measure less than 10 ng/ml (90 nM) histamine, because the slope of the standard curve is steeper, improving measurement precision below this concentration. The assays were performed in 20 μl using low-volume Cisbio plates (66PL96001) and measured using custom fluorescence filters (EX 330/80; EM 620/10 and EX 330/80; EM 665/8). Plasma was diluted using plasma sample diluent from Cisbio (62DLPDDD).

Irreversible DAO Inhibition Assay. DAO was immobilized onto high-protein-binding black fluorescence microtiter plates using a monoclonal antibody against human DAO. This process has previously been described for the development and characterization of a human DAO ELISA (Boehm et al., 2017). After washing, 0.1% HSA PBS containing a final concentration of 10 μM of the tested inhibitors was added and the wells incubated for 30 minutes at 37°. After this, the wells were washed as described in the DAO ELISA protocol (Boehm et al., 2017). H_2O_2–HRP Amplex red coupling, the most sensitive DAO activity assay, was used to measure the remaining DAO activity over 2 hours at 37°C.

Kinetic Analysis. The H_2O_2–HRP Amplex red coupling assay was used for kinetic analysis. Putrescine was tested between 5 and 80 μM and histamine between 0.63 and 10 μM. All samples were tested in duplicate, and the mean was used for further calculations. For both substrates, a DAO concentration of 200 ng/ml (1.2 nM) was used. DAO activity of the different nafamostat and substrate combinations was determined using the linear part of the slope of the increasing fluorescence signal. The coefficient of determination (R^2) of the used part of the curve was consistently above 98%. Statistical kinetic analysis was performed using GraphPad Prism.

In Silico Prediction of Nafamostat Binding to DAO. The docking preparations and experiments were performed using Maestro 2019-4 (Supplemental Refs. 5–8). The DAO structure in complex with diminazene, which is also the best resolution structure of DAO in the Protein Data Bank (PDB 3HIG), was prepared using the Protein Preparation Wizard (Supplemental Ref. 9). Nafamostat and diminazene were prepared using LigPrep (Supplemental Ref. 9). Nafamostat and diminazene dockings were performed with Glide by defining the grid in the centroid of diminazene in the B chain of the DAO crystal structure. The performance of the docking program and the best parameters (the centroid of diminazene was used as the centroid of the grid, no constraints and flexible ligand) were tested using control docking with diminazene. The control docking resulted in 6 diminazene poses (docking scores between 9.131 and −8.267) identical to the DAO/diminazene crystal structure (PDB ID 3HIG) (Supplemental Fig. 7). It also resulted in 21 similar poses among a total of 48. The same parameters were used for nafamostat docking. The interaction maps were created using the Protein–Ligand Interaction Profiler (Adasme et al., 2021). The Molecular Mechanics Generalized Born Surface Area binding energy was calculated for the diminazene/DAO complex structure (PDB ID 3HIG) and for the two best nafamostat poses obtained in the docking study (Supplemental Refs. 10 and 11). All figures were prepared using the PyMOL Molecular Graphics System, version 2.4.1, Schrödinger, LLC.

Ethics. The study numbers for the collection of plasma samples from healthy volunteers are EC:2030/2013 and EC:1810/2015. All healthy volunteers provided their informed consent before blood samples were collected. All procedures were performed in accordance with the ethical standards of the responsible committee on human experimentation (institutional and national) and with the Helsinki Declaration of 1975 (revised 2013).

Results

Nafamostat is a Potent Recombinant Human DAO Inhibitor. Using luminol with H_2O_2–HRP coupling, the IC_{50} of nafamostat for DAO inhibition is 407 nM. This is comparable to phenamil, a known DAO inhibitor (Fig. 1A) (Novotny et al., 1994). The IC_{50} of nafamostat inhibition using vanillic acid/4-aminoantipyrine H_2O_2–HRP coupling is 341 nM (Supplemental Fig. 2C). Nevertheless, potential DAO inhibitors with antioxidant activity might trap radicals released by HRP, interfering with the assay validity. We therefore tested interference of nafamostat using detection of H_2O_2 released from glucose oxidase. It is unlikely that nafamostat is a potent glucose oxidase inhibitor. Nafamostat did not block glucose oxidase activity, thus demonstrating that there is no antioxidant activity (Supplemental Fig. 2A). We also measured direct conversion of the artificial DAO substrate p-dimethylaminomethylbenzylamine to the respective aldehyde using absorption rate changes at 250 nm (Bardsley et al., 1972). The obtained data were comparable to H_2O_2–HRP coupling (Fig. 1B). Finally, fusion of deaminated autocyclized cadaverine, δ-1-piperideine, with ortho-aminobenzaldehyde (oABA) was quantified. This was performed both without and in the presence of different nafamostat concentrations. The IC_{50} was 317 nM (Fig. 1C). Camostat or Foipan tablets dissolved in water or DMSO were at least five times less potent than nafamostat, and therefore camostat was not further pursued as a DAO inhibitor (Fig. 1D). Camostat is a prodrug, and the active metabolite is likely less active compared with the parent compound.

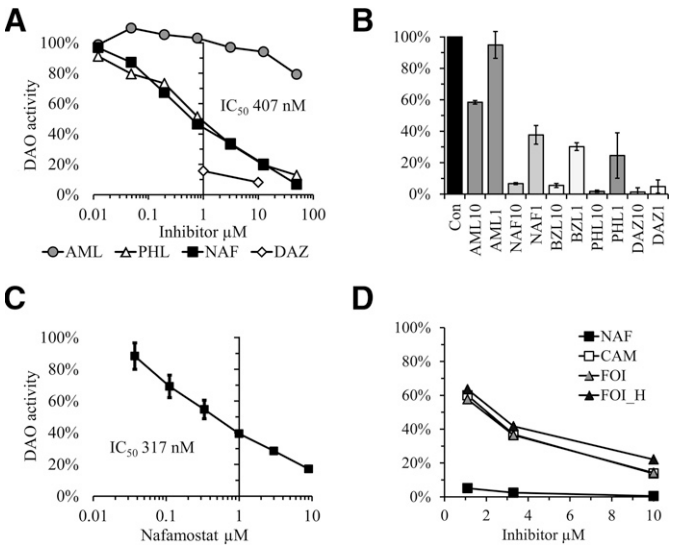

Fig. 1. Nafamostat is a potent recombinant human DAO inhibitor. (A) Nafamostat inhibits DAO activity using H_2O_2–HRP luminol coupling. One μg/ml purified DAO was incubated with 200 μM putrescine and different concentrations of various DAO inhibitors in PBS containing 0.1% HSA. The specific luminescence signals at 60 minutes were compared with DAO without inhibitors (100% DAO activity). Gray circles = AML; white triangles (Δ) = PHL; black squares (■) = NAF; white diamonds (♦) = DAZ. The means of duplicates are shown. (B) Nafamostat inhibits direct deamination of p-dimethylaminomethylbenzylamine. Aldehyde generation using 1 μg/ml recombinant human DAO was measured using specific absorption rate changes at 250 nm; The same inhibitors as in (A) including BZL were tested at 1 and 10 μM; The means (±S.E.M.) of duplicate determinations of two independent experiments are shown. (C) Nafamostat efficiently blocks the generation of δ-1-piperideine. Fusion of ortho-aminobenzaldehyde with the DAO oxidation product of cadaverine, autocyclized δ-1-piperideine, was measured using fluorescence. The slopes in the linear range were compared with different NAF concentrations and normalized to control DAO activity. The means (±S.E.M.) of two independent experiments in duplicate are shown. (D) Camostat is a weak DAO inhibitor. One, 3.3, and 10 μM CAM or Foipan tablets dissolved in DMSO (FOI) or water (FOI_H) were tested in the same assay as in (C). The means of duplicates are shown. AML, amiloride; BZL, benzamil; CAM, camostat; DAZ, diminazene aceturate; PHL, phenamil; NAF, nafamostat.

The data from three different DAO activity assays characterize nafamostat as a potent direct DAO inhibitor, excluding relevant assay interferences, possibly explaining DAO inhibition.

Nafamostat Is a Reversible DAO Inhibitor Whose Potency Is pH Independent at Physiologic pH Levels. All known irreversible DAO inhibitors like phenylhydrazine, methylhydrazine, or aminoguanidine possess a terminal hydrazine group covalently binding to the highly reactive topaquinone in the active center of DAO (Janes et al., 1992; McGrath et al., 2010). Although the potent DAO inhibitor diminazene aceturate carries an endogenous hydrazine group, it is a reversible DAO inhibitor (McGrath et al., 2009). Nafamostat does not have a hydrazine group. Nevertheless, tryptase is slowly irreversibly inhibited by nafamostat (Aoyama et al., 1984; Fujii and Hitomi, 1981). Nafamostat (and camostat) inhibition of the transmembrane protease serine 2 (TMPRSS2), involved in the cellular entry of SARS-CoV-2, seems covalent (Hempel et al., 2021). Therefore we tested whether nafamostat is an irreversible DAO inhibitor.

After washing microtiter plates with immobilized DAO, DAO activity after preincubation with 10 μM nafamostat was equivalent to wells without the addition of an inhibitor. The two hydrazine derivatives showed strong continuous DAO inhibition after the washing step, although irreversibility is not stable and DAO activity is slowly recovering (Fig. 2A). The potent DAO inhibitor diminazene rapidly dissociated from the active center, and DAO activity was immediately restored to control values after washing the wells (Fig. 2, A and B). These results strongly argue against irreversible DAO inhibition by nafamostat.

The Chemicalize software (ChemAxon) calculated a pKa of 7.6 and 8.5 for the guanidine moiety of nafamostat and camostat, respectively (data not shown). This is unusually low for a guanidine group, because guanidine shows a pKa of 12.5, similar to amidine. We therefore tested pH-dependent DAO inhibition of nafamostat using the Britton Robinson buffer system. If a double-protonated nafamostat molecule is important for inhibition, relative DAO inhibition at pH 6.0 should be stronger when compared with pH 8.0. If a single-protonated nafamostat is a better relative DAO inhibitor, nafamostat should be more potent at higher pH values. The data presented in Fig. 2C demonstrate that the pKa of the guanidine moiety is higher than 9.0. Relative DAO inhibition is constant between pH 6 and 8 and decreases afterward. This pattern is congruent with a pKa of 9.6 but not 7.6 (Fig. 2D). The pH-dependent DAO activity pattern is equivalent to published data (Elmore et al., 2002).

Nafamostat Is a Mixed-Mode DAO Inhibitor. In the next experiments, we employed kinetic analysis using different nafamostat concentrations combined with various histamine and putrescine substrate levels three- to fourfold below and above the published K_m values. The published K_m values presumed to be most reliable are 20 and 2.8 μM for putrescine and histamine, respectively (Elmore et al., 2002). We obtained nafamostat inhibition constant K_i values of 27 nM and 138 nM for putrescine and histamine respectively (Fig. 3, A and B). The ratio of the K_m to the K_i of putrescine is 741 and the equivalent histamine ratio just 20. The 37-fold difference between putrescine and histamine suggests that nafamostat is a more potent DAO inhibitor using the lower-affinity substrate putrescine compared than the higher-affinity substrate histamine. The K_i ratio of histamine to putrescine of 5.1 is similar to the K_m ratio of 7.1. The corresponding V_{max} and K_m data, including the standard errors at different nafamostat concentrations, are shown in Fig. 3, C and D. At low nafamostat concentrations, the K_m values for putrescine and histamine increase 7.1- and 8.4-fold per μM increase in nafamostat (data not shown). The IC_{50} values dependent on the substrate concentrations are shown in Fig. 3, E and F. Based on changing K_m and V_{max} values, nafamostat is likely a mixed-mode inhibitor. This hypothesis was substantiated by comparing different models of inhibition using the extra sum-of-squares F test, the most appropriate test to identify the mode of inhibition according to the GraphPad manual. These data and additional parameters obtained from kinetic analysis are summarized in Table 1.

Human Plasma Shifts the Inhibitory Potency of Nafamostat. The kinetic data imply that the assay substrate concentration will have a significant influence on the potency of nafamostat to inhibit DAO activity. Normal histamine concentrations are below 1 ng/ml (9 nM) (Kaliner et al., 1982). The mean histamine concentration during severe anaphylaxis following insect sting challenge was 140 ng/ml or 1.3 μM (van der Linden et al., 1992). The other known natural substrates of DAO are the polyamines putrescine, spermidine, and spermine,

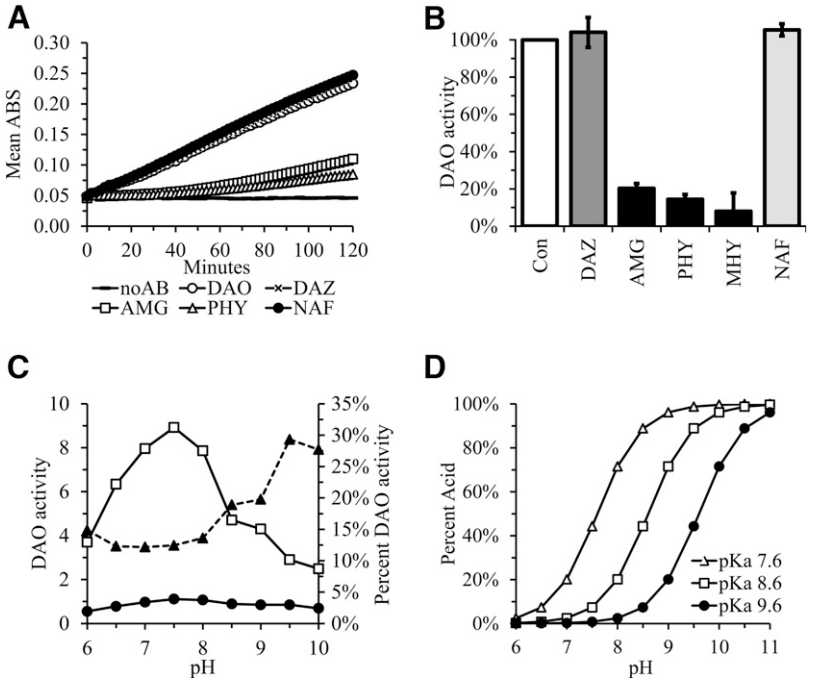

Fig. 2. Nafamostat is a reversible DAO inhibitor and pH independent at physiologically relevant pH values. (A) Nafamostat is not an irreversible DAO inhibitor. Purified DAO was immobilized on a microtiter plate precoated with a monoclonal anti-DAO antibody and incubated with various inhibitors at 10 μM. After 30 minutes at 37°C, the plates were washed and DAO activity was measured using H_2O_2–HRP vanillic acid/4-aminoantipyrine coupling. The means of duplicate determinations are shown; (B) The mean (+/−SEM) specific absorption at 60 min of 3 independent experiments as presented in (A) are summarized with n = 3 for control DAO activity (Con; 100%), NAF and DAZ and n = 1 for AMG, PHY and MHY (methylhydrazine; irreversible DAO inhibitor); For AMG, PHY and MHY the SDs of the duplicates are shown; (C) Relative DAO inhibition by NAF is equal between pH 6 and 8. The Britton Robinson buffer system was used to measure DAO activity between pH 6 and 10. White squares (□) represent DAO control oxidation rates corresponding to the slopes of chromophore accumulation using H_2O_2-HRP vanillic acid/4-aminoantipyrine coupling; Data using NAF at 1 μM are presented using black circles (●). NAF inhibition as percent of DAO activity is shown on the second y-axis (black triangles; ▲); (D) The Chemicalize software estimated a pKa of 7.6 for the guanidine moiety of NAF. The three curves were generated using the Henderson-Hasselbalch equation. Percent acid represents percent deprotonation of the guanidine moiety of NAF at different pKa values. AMG = aminoguanidine (irreversible DAO inhibitor); DAO, control wells without inhibitor; DAZ, diminazene aceturate; NAF, nafamostat; noAB, no anti-DAO antibody coating; PHY, phenylhydrazine (irreversible DAO inhibitor).

with K_m values of 20 μM, 1100 μM, and >3000 μM, respectively (Elmore et al., 2002). Nevertheless, the plasma or serum concentrations of these three polyamines are below 1 μM combined and are unlikely to significantly interfere with DAO inhibition by nafamostat (Russell, 1983).

Giardina et al. (2018) showed that at 1 nM tryptase 10% and 20% of human plasma shifts the IC_{50} values of a bivalent serine protease inhibitor 1.6- and 2.6-fold, respectively. Linear extrapolation to 100% plasma would cause an eightfold shift in the IC_{50} (Supplemental Fig. 6). The mechanism responsible for this shift was not elucidated. We used DAO at 1.2–6 nM (0.2 to 1 μg/ml) in our experiments. Finally, stability of nafamostat could influence the potency to inhibit DAO in plasma. Nafamostat is possibly hydrolyzed by esterases with a half-life of approximately 40 minutes using 100 μM nafamostat starting concentration and a rate of 6.5 μM/min, but a low K_m of 8.9 mM (Yamaori et al., 2006). At lower nafamostat concentrations, the rate is likely to be significantly reduced. Addition of 1 mM Ellman's reagent or DNT [5,5′-dithiobis(2-nitrobenzoic acid)] to plasma inhibited degradation of 500 μM nafamostat by 83% (Yamaori et al., 2006). The responsible esterase was not identified. In the following experiments we attempted to address two main questions. First, is the inhibitory potency of nafamostat reduced using the complex matrix plasma, and second, do esterase inhibitors increase the potency of nafamostat by blocking degradation using 80–90% plasma?

The highly sensitive H_2O_2–HRP Amplex red coupling assay cannot be used in plasma or serum because of the high antioxidant capacity of these complex matrices (Boehm et al., 2020). Using the recently published sensitive fluorescence assay to measure DAO activity in complex matrices like plasma or tissue extracts, we were able to reduce the substrate concentration from 200 μM to 20 μM cadaverine (Supplemental Fig. 3). The IC_{50} in 85% plasma shifted from 2.3 μM to 386 nM, a sixfold drop, after reducing cadaverine 10-fold from 200 to 20 μM (Fig. 4A) (Boehm et al., 2020). Lower substrate concentrations cannot be used because of assay sensitivity limitations. Addition of 1 or 2 mM DNT did not influence the IC_{50} values of DAO inhibition by nafamostat (Fig. 4B). Camostat is also hydrolyzed by plasma esterases and sodium fluoride inhibited camostat degradation (Midgley et al., 1994), but no effect was measured using 40 mM NaF in our assay (Supplemental Fig. 5B). We also tested 2-hydroxyquinoline (2HQ), a potent arylesterase inhibitor (Khersonsky and Tawfik, 2005), but did not see any effect on DAO inhibition (Supplemental Fig. 5B). Finally, we reasoned that high concentrations of naphthalen-2-yl benzoate might occupy the responsible enzymes potentiating nafamostat inhibition. Naphthalen-2-yl benzoate corresponds to nafamostat without both the terminal amidinium and guanidinium moieties. Diamine oxidase inhibition was not increased using 1 mM naphthalen-2-yl benzoate (Supplemental Fig. 5A). The influence of the different (aryl)esterase inhibitors on DAO activity measurements was within acceptable boundaries (Supplemental Fig. 4).

Although the IC_{50} values shifted sixfold after reducing the substrate concentrations from 200 to 20 μM cadaverine, the IC_{50} values were still at least 10-fold higher compared with the K_i of 27 nM for putrescine. In general, putrescine and cadaverine behave very similarly as DAO substrate. We also tested 0.9 μM (100 ng/ml) and 0.18 μM (20 ng/ml) histamine substrate concentrations and the IC_{50}s were approximately 2 to 3 μM, which is 15- to 22-fold above the K_i of 138 nM (Fig. 4D). Lower histamine concentrations cannot be accurately quantified, because plasma must be diluted to avoid matrix effects. No histamine degradation was measured without addition of DAO (data not shown) and endogenous histamine was below 10 nM (data not shown).

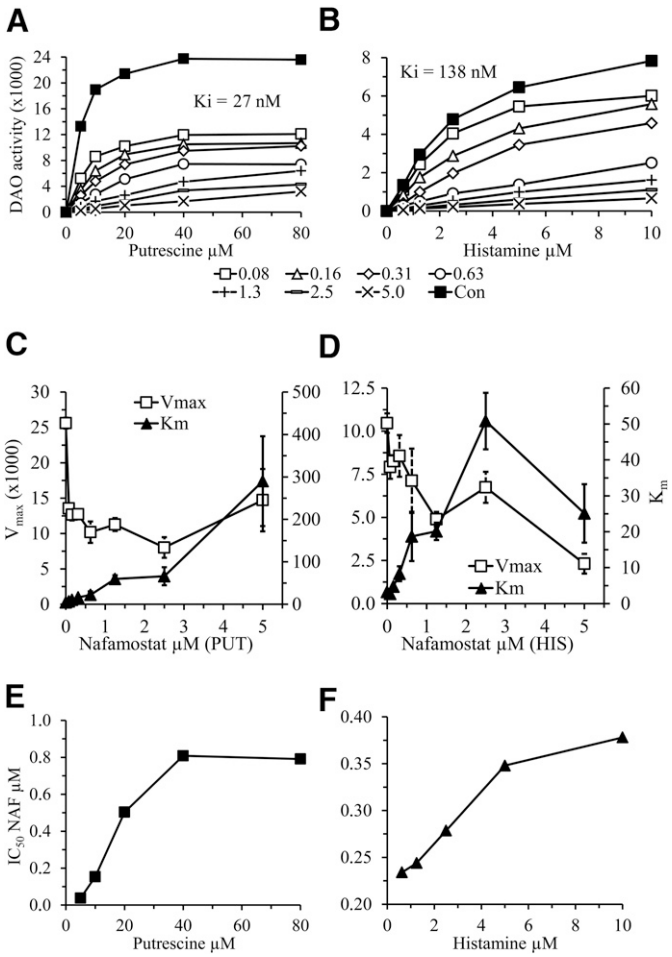

Fig. 3. Kinetic analysis of DAO inhibition by nafamostat. (A) Different putrescine concentrations were incubated with various nafamostat concentrations shown below Panels A and B; DAO activity was measured using the highly sensitive H_2O_2–HRP Amplex red coupling and corresponds to the linear part of the slope of fluorescence curves. (B) Same as in (A) using different histamine concentrations. K_i values were determined using GraphPad; the curves in (A) and (B) represent the means of duplicate determinations. (C and D) V_{max} (white squares □) and K_m (black triangles ▲) values using different nafamostat and putrescine (C) or histamine (D) concentrations; The error bars correspond to the standard error. (E) Calculated IC_{50} values are plotted versus putrescine concentrations. (F) Same as in (E) for histamine; K_i, K_m and V_{max} data and mode of inhibition are summarized in Table 1.

In Silico Docking Predicts Nafamostat Binding to DAO Similar to Diminazene. Crystal structures of two potent diamidine-type DAO inhibitors, pentamidine and diminazene, complexed with DAO have been published (PDB IDs 3HII, 3HIG). Both are mixed-mode inhibitors similar to nafamostat, which may use similar amino acids for tight binding. Nevertheless, nafamostat is not a strict diamidine because it carries a terminal amidinium and a terminal guanidinium moiety. Unlike diminazene and pentamidine, it is not symmetrical because it contains a single naphthalene double aromatic ring structure linked to the terminal amidine group (Supplemental Fig. 1). Therefore, it is possible that nafamostat might prefer only one orientation for DAO binding. We used in silico docking to predict amino acid interactions and the preferred orientation for nafamostat binding. Nafamostat docking resulted in six poses, and three of them had a binding mode similar to the binding mode of diminazene in the crystal complex (PDB ID 3HIG). The aromatic rings of two similar poses with the docking scores of −7.893 and −6.910 superimposed well with those of diminazene in the DAO complex structure (Fig. 5A). In the crystal complex (Fig. 5B) the buried amidinium group of diminazene interacts with the catalytic Asp373, and the vicinal phenyl group pi-stacks with Tyr371 and Trp376. The nitrogen atoms in the triazine make hydrogen bonds with Asp186 and Tyr148. The Tyr148 residue also pi-stacks with the distal phenyl ring, which is clamped between Tyr148 and Phe435 from the other chain. The terminal amidinium forms a water-mediated hydrogen bond with Thr145. The binding site is surrounded by the hydrophobic Val458 and Ala149 residues and the aromatic residues Tyr459, Phe184, and Tyr152.

Based on the interaction analysis (Fig. 5, C and D) the second-best pose for nafamostat showed more interactions than the best pose. Because it also showed a better calculated binding energy ΔG of −67.00 kcal/mol (the best post demonstrated a ΔG of −63.09 kcal/mol), the second pose was selected as a representative binding mode for nafamostat. Like the buried amidinium in the diminazene crystal complex (Fig. 5B), the buried guanidino group in the second nafamostat pose (Fig. 5C) forms a salt bridge with a catalytic Asp373, and the vicinal phenyl group pi-stacks with Tyr371 and interacts with Trp376. Compared with amidinium, the guanidinium group in nafamostat possesses an additional nitrogen, which makes both direct and water-mediated hydrogen bonds to Asn460. Like the phenyl group in diminazene, the naphtyl group in nafamostat pi-stacks with Tyr148 and interacts with Phe435 from the other chain. The central carbonyl group creates a hydrogen bond with Tyr148, and the distal amidinium interacts with Thr145 via a direct hydrogen bond and forms water-mediated hydrogen bonds with Tyr152 and Ala149. The predicted binding mode of nafamostat to DAO is highly similar to the binding mode of diminazene in the crystal complex with a

TABLE 1
Nafamostat is a mixed-mode inhibitor of human DAO using putrescine and histamine as substrates

	PUT MM Inh	S.E.	L 95% CI	U 95% CI	HIS MM Inh	SE	L 95% CI	U 95% CI
V_{max}	23111	1381	20309	25912	10126	463	9185	11066
K_i nM	27	12	3	50	138	25	87	190
K_m μM	3.1	1.1	0.9	5.3	2.8	0.34	2.1	3.5
Adj. R^2	0.926				0.986			
α	12.1				4.9			
ExSOS F	MM versus	C	0.0022				0.0006	
		NonC	0.0018				0.0003	
		UnC	0.0001				0.0001	

Adj., adjusted; C, competitive; CI, confidence interval; ExSOS F, extra sum-of-squares F test; HIS, histamine; Inh, inhibitor; L, lower; MM, mixed mode inhibition; NonC, noncompetitive; PUT, putrescine; U, upper; UnC, uncompetitive inhibition.

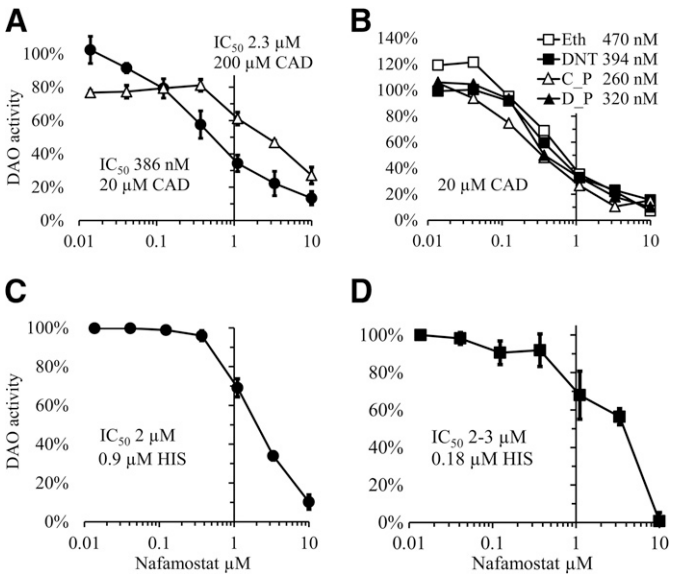

Fig. 4. Nafamostat inhibition of DAO activity in human EDTA plasma. In Panels A and B, fusion of orthoaminobenzaldehyde with autocyclized δ-1-piperideine, the cadaverine (CAD) DAO oxidation product, was measured using fluorescence. (A) 85% EDTA plasma was incubated for 1 hour at 37°C with 0.4 μg/ml purified DAO in the absence and presence of different nafamostat concentrations using 200 μM CAD (white triangles Δ; $n = 1$) and 20 μM CAD (black circles ●; $n = 4$) as indicated. Specific fluorescence was normalized to control DAO samples. The means (±coefficient of variation for 200 μM CAD and ±S.D. for 20 μM CAD) of duplicate determinations are shown. (B) Similar conditions to Panel A but incubation was only performed for 30 minutes at 37°C. DNT, 5,5′-dithiobis(2-nitrobenzoic acid) or Ellman's reagent was used at 1 mM; Eth means 5% ethanol (DNT solvent); C_P means control plasma and D_P means DNT directly dissolved in control plasma at 2 mM. Only 80% plasma was used in the Eth and DNT samples. The numbers after the sample abbreviations are IC_{50} concentrations. The means of duplicates of single donors for each set (ethanol as solvent with and without DNT vs. direct dissolution of DNT in plasma) are shown. (C and D) 90% EDTA plasma was spiked with 1 μg/ml (6 nM) purified DAO and 100 ng/ml (0.9 μM) or 20 ng/ml (0.18 μM) histamine in the absence and presence of different nafamostat concentrations. After 1 hour's incubation at 37°C, the remaining histamine was quantified using the Cisbio HTRF histamine assay. The means (±S.D.) of four different plasma samples from healthy volunteers are shown in Panels C and D. Histamine measurements were performed in duplicate. DAO activity in the absence of nafamostat was set to 100%.

preferred orientation of the guanidinium group toward the topaquinone.

Discussion

It is not surprising that nafamostat is a potent DAO inhibitor when one compares nafamostat with the structure of the known DAO inhibitors pentamidine and diminazene. In silico ligand docking studies revealed a remarkable similarity in amino acid interactions between nafamostat and diminazene. The K_i of diminazene using insect cell–derived DAO and putrescine was 14 nM and therefore quite similar to the 27 nM measured in our experiments (McGrath et al., 2009).

The fivefold increased K_i for histamine (138 nM) compared with putrescine (27 nM) is likely a reflection of the seven times lower K_m of histamine (2.8 μM) compared with putrescine (20 μM) for DAO (Elmore et al., 2002). We have seen similarly higher IC_{50} values for histamine compared with the simple diamines putrescine or cadaverine using other inhibitors (unpublished data). Nafamostat is clearly a potent DAO inhibitor in vitro, but the key question is whether DAO inhibition could be involved in the hypersensitivity reactions during nafamostat treatment and possibly also in effects currently ascribed to protease inhibition in animal models or clinical trials. Therefore, nafamostat inhibition of histamine degradation in plasma is more important, and here we measured IC_{50} values of 2–3 μM using 180 nM histamine.

Normal histamine concentrations are below 0.5 ng/ml or 4.5 nM (Pollock et al., 1991). Histamine starts to induce symptoms such as flush and headache at less than 3 ng/ml, and significant hypotension develops above 5 ng/ml (Kaliner et al., 1982; Pollock et al., 1991). We could not test lower histamine concentrations in our DAO activity assays, but during severe anaphylaxis, mean histamine concentrations of 140 ng/ml or 1260 nM have been measured, and at this level, 2–3 μM nafamostat would be sufficient to inhibit plasma DAO activity (Van der Linden et al., 1992). Table 2 summarizes published IC_{50} and K_i data for nafamostat using frequently pure buffer matrices or more than fivefold diluted plasma samples. Hitomi et al. (1985) and Fujii and Hitomi (1981) published ratios of IC_{50} to K_i values of 0.68 and 0.39 respectively for prothrombin, which circulates at 1.4 μM. In our case the ratio of IC_{50} using 90% plasma to K_i in buffer for histamine is 22-fold. Giardina et al. (2018) published an extrapolated IC_{50} shift for tryptase inhibition of at least sevenfold comparing buffer with >80% plasma (Supplemental Fig. 6). Protease inhibition assays with nafamostat might show significantly higher IC_{50} values, indicating weaker potency of nafamostat using high plasma concentrations. Pâques and Römisch (1991) used 75% plasma to test coagulation parameters, and the K_i values seem higher compared with the other data in Table 2. Published nafamostat inhibition data are inconsistent (Table 2 and Supplemental Table 2). What might be the reason for this strong shift in the plasma IC_{50} values when using plasma versus buffer?

We initially assumed that nafamostat is rapidly degraded by abundant plasma arylesterases but we were not able to find any effect of several arylesterase inhibitors on DAO inhibition using nafamostat (Yamaori et al., 2006). An alternative explanation would be that plasma proteins trap nafamostat and therefore the IC_{50} values increase. Table 2 lists the concentrations of nafamostat target proteases. The sum of the known nafamostat-binding proteins is approximately 5 μM. Nafamostat might bind to these proteins with significant affinity before the proteases are activated.

In our assays, we used maximally 12 nM DAO concentrations, and therefore the ratio of all nafamostat-binding proteins to DAO would be 417. This indicates that nafamostat binding to DAO competes with binding to 400-fold more abundant additional target proteins. Plasma DAO might be significantly inhibited at the high nafamostat concentrations used during hemodialysis or cardiopulmonary bypass operations with saturation of protease-binding sites.

Some of the SARS-CoV-2 cell entry inhibition data have been performed with buffer or only 10% plasma. The relatively low IC_{50} values of 55 nM (Hempel et al., 2021) or 10 nM (Yamamoto et al., 2020) might increase significantly using higher plasma concentrations, but irreversible binding likely follows different inhibition kinetics.

Normally, human DAO is not circulating but is present at high local concentrations in the extracellular matrix of the jejunum/ileum and renal proximal tubular epithelial cells (Boehm et al., 2017). Nevertheless, exogenous high molecular/unfractionated

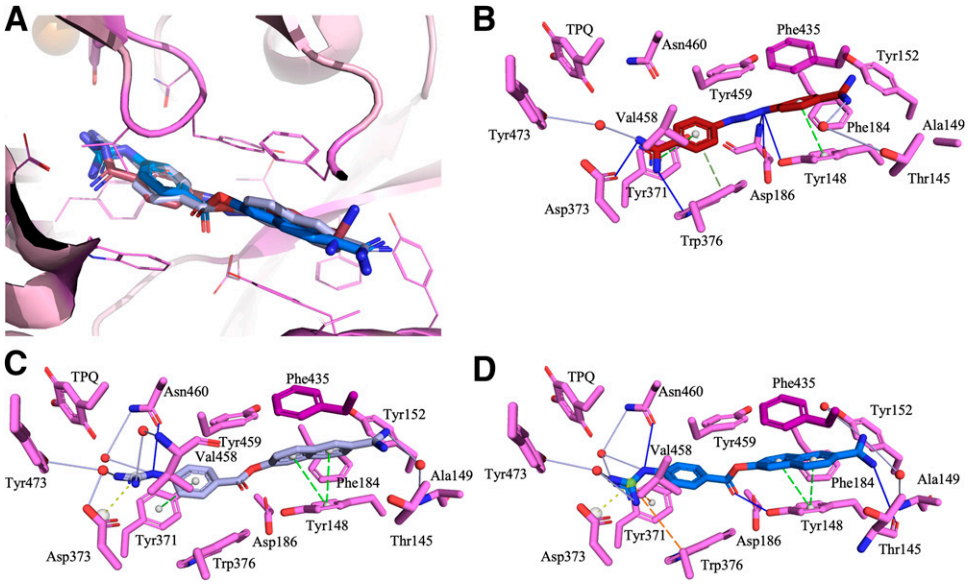

Fig. 5. Molecular docking of nafamostat to the active site of DAO compared with the diminazene/DAO crystal structure. All atomic interactions are presented based on the results from the PLIP webserver (Adasme et al., 2021). The side chains for the residues in chain A within 4Å from the binding site are shown as violet lines in Panel A and as sticks in Panels B to D. Phe435 from chain B is purple. (A) Diminazene (light red) in complex with DAO (PDB ID 3HIG, red) superimposed with the two best poses of docked nafamostat (light and dark blue). (B) The interactions between diminazene (red) and DAO in the crystal complex. (C) The interactions between the best pose of nafamostat (light blue) docking with DAO. (D) The interactions between the second best pose of nafamostat (dark blue) docking with DAO.

heparin is able to rapidly release DAO from the extracellular storage sites in the gastrointestinal tract (D'Agostino et al., 1988). During cardiopulmonary bypass operations with or without nafamostat treatment, heparin was used at 300 IU/kg, and this amount of heparin very likely released endogenous DAO (Miyamoto et al., 1992; D'Agostino et al., 1988). Nafamostat, probably present at μM plasma concentrations during the cardiopulmonary bypass procedure, might have mediated inhibition of heparin-released plasma DAO, and this inhibition could have caused the more than fivefold difference in plasma histamine concentrations (Miyamoto et al., 1992).

Diamine oxidase is also released into plasma during severe anaphylaxis and mast cell activation events in both animals and humans (Rose and Leger, 1952; Code et al., 1961; Boehm et al., 2019). Therefore, nafamostat could cause anaphylaxis and mast cell activation events to deteriorate by blocking plasma DAO activity. Recombinant human DAO might also be developed as a new first-in-class biopharmaceutical for the treatment of anaphylaxis, mastocytosis, chronic urticaria, or asthma exacerbations (Gludovacz et al., 2021). Coadministration of nafamostat might interfere with the potency of recombinant human DAO.

High concentrations of DAO are bound extracellularly to interstitial heparan sulfate proteoglycans in the gastrointestinal tract and renal proximal tubular cells, but the role of DAO in the degradation of endogenous histamine released during anaphylaxis is not clear. Nevertheless, if the concentration of nafamostat in the interstitial fluid is high enough to efficiently inhibit local matrix-bound DAO, higher histamine concentrations are not only locally present after release from degranulating mast cells but will also reach the circulation. Locally and systemically elevated histamine levels will increase clinical symptom severity during anaphylaxis, mast cell activation syndrome, mastocytosis, or chronic urticaria. Of the approximately 100 mg total histamine stored in the body, 50% and 30% are located within the granules of the mast cells in the

TABLE 2

Nafamostat-binding proteins in competition with DAO binding

The different plasma protease activities have been measured after generation of active proteases; Nafamostat binding data to the not-activated enzyme precursors are not available.

NBP	[Plasma] μM	IC_{50} Hitomi et al. (1985)	K_i Hitomi et al. (1985)	IC_{50} Fujii and Hitomi (1981)	K_i Fujii and Hitomi (1981)	IC_{50} Aoyama et al. (1984)	K_i Pâques and Römisch (1991)	IC_{50} Giardina et al. (2018)
PK	0.24	3.0×10^{-9}		3.1×10^{-7}		3.9×10^{-6}	1.2×10^{-8}	2.0×10^{-10}
Plg	2.2	1.0×10^{-7}		4.1×10^{-7}		1.2×10^{-7}	3.7×10^{-6}	3.7×10^{-9}
PT	1.4	8.8×10^{-7}	1.3×10^{-6}	3.3×10^{-7}	8.4×10^{-7}	1.9×10^{-6}	4.9×10^{-6}	2.3×10^{-7}
FXII	0.44	3.3×10^{-7}					1.1×10^{-7}	
FX	0.13	2.1×10^{-6}	4.1×10^{-6}				1.2×10^{-4}	8.8×10^{-7}
C1r	0.39			2.1×10^{-7}	1.4×10^{-8}	8.0×10^{-7}		
C1s	0.41			5.1×10^{-8}	3.8×10^{-8}	2.9×10^{-8}		
Sum	5.2							
The following data are from this study								
[DAO][a] μg/ml	[DAO][a] μM	Ki PUT	Ki HIS	IC_{50} PUT[b]	IC_{50} PUT[b]	IC_{50} CAD[b]		
0.4	0.0048	2.7×10^{-8}	1.4×10^{-7}	4.1×10^{-7}	3.4×10^{-7}	3.2×10^{-7}		
1	0.012							

C1r and C1s, complement component 1r and 1s; CAD, cadaverine; FXII, factor XII; HIS, histamine; IC_{50}, inhibitory concentration 50%; K_i, inhibitor constant; NBP, potential nafamostat-binding protein; Plg, plasminogen; PK, pre-Kallikrein; PT, prothrombin; PUT, putrescine.

[a]DAO concentrations used in this study.

[b]200 μM substrate concentration.

gastrointestinal tract and the skin, respectively. It is these organs that frequently demonstrate symptoms during hypersensitivity reactions (Boehm et al., 2021).

The interstitial fluid contains about 30% of the protein concentration compared with plasma (Supplemental Table 1) (Fogh-Andersen et al., 1995) and therefore, simplified, the concentration of nafamostat-binding proteins might be only about 1.5 μM, and this could increase the potency of nafamostat to inhibit local DAO activity in the gastrointestinal tract and kidneys.

What are the concentrations of nafamostat in the interstitial fluid or in the gastrointestinal tract and kidneys? The volume of distribution for nafamostat in healthy volunteers was described as 0.36 L/kg or 25 L in a person weighing 70 kg, indicating that nafamostat is present at high concentrations in the interstitial fluid (Osono et al., 1991). The interstitial fluid compartment is about three times the plasma volume. In rats, 15 minutes after intravenous infusion, nafamostat rapidly accumulated in the kidneys and duodenum/jejunum (65- and 8- to 10-fold, respectively, compared with plasma). It might then be reabsorbed in the kidneys in the proximal tubules via organic cation transporters (Supplemental Tables 3 and 4) (Nanpo et al., 1984; Li et al., 2004). Pentamidine and furamidine, two diamidines with related chemical structures compared with nafamostat, are also transported via human organic cation transporters (Ming et al., 2009). Diamine oxidase is located in the extracellular matrix of renal proximal tubular and gastrointestinal epithelial cells. If humans show a similar accumulation of nafamostat when compared with rats, DAO might be potently inhibited by the high tissue concentrations of nafamostat. Nafamostat might compete with the transport of histamine into basophils or other cells. Histamine also uses organic cation transporters, and if high plasma nafamostat concentrations interfere with histamine reabsorption into basophils, and possibly endothelial cells and other cells, the relative histamine exposure would increase (Schneider et al., 2005; Sakata et al., 2010).

Nafamostat is clearly associated with hypersensitivity reactions in humans, but is there additional in vivo evidence of DAO inhibition and consequently of elevated histamine concentrations? High-dose nafamostat administration in dogs, defined as plasma concentrations of more than 15 μM for 24 hours, caused the mean arterial pressure to drop statistically significantly after 6 hours and remain low until the end of the infusions 18 hours later (Okamoto et al., 1994). The mean arterial pressure decrease was approximately 35%, from 125 to 80 mm Hg. DAO inhibition at these high nafamostat concentrations could have increased the circulating histamine levels and at least cocontributed to hypotension in dogs, which are sensitive to histamine (Owen et al., 1982).

Ceuleers et al. (2018) tested three nafamostat concentrations (0.1, 1, and 10 mg/kg) in a rat colitis model for irritable bowel syndrome. Tryptase, a biomarker for mast cells, was increased during inflammation, indicating the involvement of mast cells. Although nafamostat is a highly potent inhibitor for tryptase, only the lower nafamostat concentration showed beneficial effects in this model. Interestingly, experimental colitis in mice seems to be driven by histamine released from mast cells via histamine 4 receptor binding (Wechsler et al., 2018). We speculate that medium and high nafamostat concentrations not only inhibited tryptase but also local DAO, thus resulting in elevated proinflammatory histamine concentrations counteracting the positive effects of tryptase inhibition.

In conclusion, nafamostat is a potent DAO inhibitor. During anaphylaxis or in general mast cell activation with massive release of histamine, concomitant nafamostat treatment might cause potent DAO inhibition leading to elevated histamine levels with possibly life-threatening consequences.

Acknowledgments

The authors thank three diploma students, Julia Henkel, Linda Thurner, and Marija Gorickic, for performing some of the experiments used in this publication. The library at the MUV was indispensable for providing literature. The authors also thank the bioinformatics (J.V. Lehtonen), translational activities and structural biology (FINStruct) infrastructure support from the Biocenter Finland and the computational infrastructure support from the CSC IT Center for Science at the Structural Bioinformatics Laboratory (SBL) of the Åbo Akademi University. The SBL is part of the NordForsk Nordic POP (Patient Oriented Products) and the Solutions for Health strategic area of the Åbo Akademi University. The authors are indebted to Sarah Ely for the final polish in the proper usage of the English language.

Authorship Contributions

Participated in research design: Boehm, Jilma.
Conducted experiments: Petroczi, Gludovacz, Alix, Vakal.
Performed data analysis: Boehm, Alix, Vakal, Salminen.
Wrote or contributed to the writing of the manuscript: Boehm, Borth, Salminen, Jilma.

References

Adasme MF, Linnemann KL, Bolz SN, Kaiser F, Salentin S, Haupt VJ, and Schroeder M (2021) PLIP 2021: expanding the scope of the protein-ligand interaction profiler to DNA and RNA. *Nucleic Acids Res* **49**:W530–W534.
Aoyama T, Ino Y, Ozeki M, Oda M, Sato T, Koshiyama Y, Suzuki S, and Fujita M (1984) Pharmacological studies of FUT-175, nafamstat mesilate. I. Inhibition of protease activity in in vitro and in vivo experiments. *Jpn J Pharmacol* **35**:203–227.
Asakura H and Ogawa H (2020) Potential of heparin and nafamostat combination therapy for COVID-19. *J Thromb Haemost* **18**:1521–1522.
Bardsley WG, Crabbe MJ, Shindler JS, and Ashford JS (1972) Oxidation of p-dimethylaminomethylbenzylamine by pig kidney diamine oxidase. A new method for spectrophotometric assay. *Biochem J* **127**:875–879.
Boehm T, Karer M, Gludovacz E, Petroczi K, Resch M, Schuetzenberger K, Klavins K, Borth N, and Jilma B (2020) Simple, sensitive and specific quantification of diamine oxidase activity in complex matrices using newly discovered fluorophores derived from natural substrates. *Inflamm Res* **69**:937–950.
Boehm T, Pils S, Gludovacz E, Szoelloesi H, Petroczi K, Majdic O, Quaroni A, Borth N, Valent P, and Jilma B (2017) Quantification of human diamine oxidase. *Clin Biochem* **50**:444–451.
Boehm T, Reiter B, Ristl R, Petroczi K, Sperr W, Stimpfl T, Valent P, and Jilma B (2019) Massive release of the histamine-degrading enzyme diamine oxidase during severe anaphylaxis in mastocytosis patients. *Allergy* **74**:583–593.
Boehm T, Ristl R, Joseph S, Petroczi K, Klavins K, Valent P, and Jilma B (2021) Metabolome and lipidome derangements during a severe mast cell activation event in a patient with indolent systemic mastocytosis. *J Allergy Clin Immunol* **148**:1533–1544.
Ceuleers H, Hanning N, Heirbaut J, Van Remoortel S, Joossens J, Van Der Veken P, Francque SM, De Bruyn M, Lambeir AM, De Man JG, et al. (2018) Newly developed serine protease inhibitors decrease visceral hypersensitivity in a post-inflammatory rat model for irritable bowel syndrome. *Br J Pharmacol* **175**:3516–3533.
Code CF, Cody DT, Hurn M, Kennedy JC, and Strickland MJ (1961) The simultaneous release of histamine and a histamine-destroying factor during anaphylaxis in rats. *J Physiol* **156**:207–216.
D'Agostino L, Daniele B, Pallone F, Pignata S, Leoni M, and Mazzacca G (1988) Postheparin plasma diamine oxidase in patients with small bowel Crohn's disease. *Gastroenterology* **95**:1503–1509.
Duch DS, Bacchi CJ, Edelstein MP, and Nichol CA (1984) Inhibitors of histamine metabolism in vitro and in vivo. Correlations with antitrypanosomal activity. *Biochem Pharmacol* **33**:1547–1553.
Elmore BO, Bollinger JA, and Dooley DM (2002) Human kidney diamine oxidase: heterologous expression, purification, and characterization. *J Biol Inorg Chem* **7**:565–579.
Fogh-Andersen N, Altura BM, Altura BT, and Siggaard-Andersen O (1995) Composition of interstitial fluid. *Clin Chem* **41**:1522–1525.

Fujii S and Hitomi Y (1981) New synthetic inhibitors of C1r, C1 esterase, thrombin, plasmin, kallikrein and trypsin. *Biochim Biophys Acta* **661**:342–345.
Giardina SF, Werner DS, Pingle M, Bergstrom DE, Arnold LD, and Barany F (2018) A novel, nonpeptidic, orally active bivalent inhibitor of human β-tryptase. *Pharmacology* **102**:233–243.
Gludovacz E, Schuetzenberger K, Resch M, Tillmann K, Petroczi K, Schosserer M, Vondra S, Vakal S, Klanert G, Pollheimer J, et al. (2021) Heparin-binding motif mutations of human diamine oxidase allow the development of a first-in-class histamine-degrading biopharmaceutical. *eLife* **10**:e68542.
Han SJ, Kim HS, Kim KI, Whang SM, Hong KS, Lee WK, and Lee SH (2011) Use of nafamostat mesilate as an anticoagulant during extracorporeal membrane oxygenation. *J Korean Med Sci* **26**:945–950.
Hempel T, Raich L, Olsson S, Azouz NP, Klingler AM, Hoffmann M, Pöhlmann S, Rothenberg ME, and Noé F (2021) Molecular mechanism of inhibiting the SARS-CoV-2 cell entry facilitator TMPRSS2 with camostat and nafamostat. *Chem Sci (Camb)* **12**:983–992.
Hitomi Y, Ikari N, and Fujii S (1985) Inhibitory effect of a new synthetic protease inhibitor (FUT-175) on the coagulation system. *Haemostasis* **15**:164–168.
Hoffmann M, Schroeder S, Kleine-Weber H, Müller MA, Drosten C, and Pöhlmann S (2020) Nafamostat mesylate blocks activation of SARS-CoV-2: New treatment option for COVID-19. *Antimicrob Agents Chemother* **64**:e00754-20.
Janes SM, Palcic MM, Scaman CH, Smith AJ, Brown DE, Dooley DM, Mure M, and Klinman JP (1992) Identification of topaquinone and its consensus sequence in copper amine oxidases. *Biochemistry* **31**:12147–12154.
Kaliner M, Shelhamer JH, and Ottesen EA (1982) Effects of infused histamine: correlation of plasma histamine levels and symptoms. *J Allergy Clin Immunol* **69**:283–289.
Khersonsky O and Tawfik DS (2005) Structure-reactivity studies of serum paraoxonase PON1 suggest that its native activity is lactonase. *Biochemistry* **44**:6371–6382.
Kim HS, Lee KE, Oh JH, Jung CS, Choi D, Kim Y, Jeon JS, Han DC, and Noh H (2016) Cardiac arrest caused by nafamostat mesilate. *Kidney Res Clin Pract* **35**:187–189.
Kim JH, Park JY, Jang SH, Kim JK, Song YR, Lee HS, and Kim SG (2021) Fatal anaphylaxis due to nafamostat mesylate during hemodialysis. *Allergy Asthma Immunol Res* **13**:517–519.
Li Q, Sai Y, Kato Y, Muraoka H, Tamai I, and Tsuji A (2004) Transporter-mediated renal handling of nafamostat mesilate. *J Pharm Sci* **93**:262–272.
Maruyama H, Miyakawa Y, Gejyo F, and Arakawa M (1996) Anaphylactoid reaction induced by nafamostat mesilate in a hemodialysis patient. *Nephron* **74**:468–469.
McGrath AP, Caradoc-Davies T, Collyer CA, and Guss JM (2010) Correlation of active site metal content in human diamine oxidase with trihydroxyphenylalanine quinone cofactor biogenesis. *Biochemistry* **49**:8316–8324.
McGrath AP, Hilmer KM, Collyer CA, Shepard EM, Elmore BO, Brown DE, Dooley DM, and Guss JM (2009) Structure and inhibition of human diamine oxidase. *Biochemistry* **48**:9810–9822.
Midgley I, Hood AJ, Proctor P, Chasseaud LF, Irons SR, Cheng KN, Brindley CJ, and Bonn R (1994) Metabolic fate of ^{14}C-camostat mesylate in man, rat and dog after intravenous administration. *Xenobiotica* **24**:79–92.
Minakata D, Fujiwara SI, Ikeda T, Kawaguchi SI, Toda Y, Ito S, Ochi SI, Nagayama T, Mashima K, Umino K, et al. (2019) Comparison of gabexate mesilate and nafamostat mesilate for disseminated intravascular coagulation associated with hematological malignancies. *Int J Hematol* **109**:141–146.
Ming X, Ju W, Wu H, Tidwell RR, Hall JE, and Thakker DR (2009) Transport of dicationic drugs pentamidine and furamidine by human organic cation transporters. *Drug Metab Dispos* **37**:424–430.
Miyamoto Y, Nakano S, Kaneko M, Takano H, and Matsuda H (1992) Clinical evaluation of a new synthetic protease inhibitor in open heart surgery. Effect on plasma serotonin and histamine release and blood conservation. *ASAIO J* **38**:M395–M398.
Mori S, Itoh Y, Shinohata R, Sendo T, Oishi R, and Nishibori M (2003) Nafamostat mesilate is an extremely potent inhibitor of human tryptase. *J Pharmacol Sci* **92**:420–423.
Nanpo T, Ohtsuki T, Jin Y, Matsunaga K, Takahashi M, Shibuya M, Sasaki H, and Kurumi M (1984) Pharmacokinetic study of FUT-175 (nafamostat mesilate). (1) Blood level profiles, tissue distribution, metabolism and excretion in rats after intravenous administration. *Clin Rep* **18**:467–488.
Novotny WF, Chassande O, Baker M, Lazdunski M, and Barbry P (1994) Diamine oxidase is the amiloride-binding protein and is inhibited by amiloride analogues. *J Biol Chem* **269**:9921–9925.
Okajima K, Uchiba M, and Murakami K (1995) Nafamostat mesilate. *Cardiovasc Drug Rev* **13**:51–65.
Okamoto T, Mizoguchi S, Terasaki H, and Morioka T (1994) Safety of high-dose of nafamostat mesilate: toxicological study in beagles. *J Pharmacol Exp Ther* **268**:639–644.
Ookawara S, Ito K, and Morishita Y (2018) Sustained deterioration of hepatic oxygenation after nafamostat mesilate-induced anaphylactic shock during hemodiafiltration. *Artif Organs* **42**:674–675.
Osono E, Takeuchi M, Kitamura H, Matsunobu S, Komaba Y, Aoyama T, Kawabe M, Arai T, Lino Y, Hara K, et al. (1991) Pharmacokinetics of nafamostat mesilate (FUT) in patients undergoing hemodialysis [in Japanese]. *Dialysis J* **24**:49–53.
Owen DA, Harvey CA, and Boyce MJ (1982) Effects of histamine on the circulatory system. *Klin Wochenschr* **60**:972–977.
Påques EP and Römisch J (1991) Comparative study on the in vitro effectiveness of antithrombotic agents. *Thromb Res* **64**:11–21.
Pollock I, Murdoch RD, and Lessof MH (1991) Plasma histamine and clinical tolerance to infused histamine in normal, atopic and urticarial subjects. *Agents Actions* **32**:359–365.
Rose B and Leger J (1952) Serum histaminase during rabbit anaphylaxis. *Proc Soc Exp Biol Med* **79**:379–381.
Russell DH (1983) Clinical relevance of polyamines. *Crit Rev Clin Lab Sci* **18**:261–311.
Sakamoto T, Kano H, Miyahara S, Inoue T, Izawa N, Gotake Y, Matsumori M, Okada K, and Okita Y (2014) Efficacy of nafamostat mesilate as anticoagulation during cardiopulmonary bypass for early surgery in patients with active infective endocarditis complicated by stroke. *J Heart Valve Dis* **23**:744–751.
Sakata T, Anzai N, Kimura T, Miura D, Fukutomi T, Takeda M, Sakurai H, and Endou H (2010) Functional analysis of human organic cation transporter OCT2 (SLC22A3) polymorphisms. *J Pharmacol Sci* **113**:263–266.
Sattler J, Häfner D, Klotter HJ, Lorenz W, and Wagner PK (1988) Food-induced histaminosis as an epidemiological problem: plasma histamine elevation and haemodynamic alterations after oral histamine administration and blockade of diamine oxidase (DAO). *Agents Actions* **23**:361–365.
Sawada K, Ohdo M, Ino T, Nakamura T, Numata T, Shibata H, Sakou J, Kusada M, and Hibi T (2016) Safety and tolerability of nafamostat mesilate and heparin as anticoagulants in leukocytapheresis for Ulcerative Colitis: Post hoc analysis of alarge-scale,prospective,observationalstudy.*TherApherDial***20**:197–204.
Schneider E, Machavoine F, Pléau JM, Bertron AF, Thurmond RL, Ohtsu H, Watanabe T, Schinkel AH, and Dy M (2005) Organic cation transporter 3 modulates murine basophil functions by controlling intracellular histamine levels. *J Exp Med* **202**:387–393.
Schwelberger HG, Hittmair A, and Kohlwein SD (1998a) Analysis of tissue and subcellular localization of mammalian diamine oxidase by confocal laser scanning fluorescence microscopy. *Inflamm Res* **47**:S60–S61.
Schwelberger HG, Stalzer B, Maier H, and Bodner E (1998b) Expression and cellular localisation of diamine oxidase in the gastrointestinal tract of pigs. *Inflamm Res* **47**:S62–S63.
Sjaastad ÖV (1967) Potentiation by aminoguanidine of the sensitivity of sheep to histamine given by mouth. Effect of amino-guanidine on the urinary excretion of endogenous histamine. *Q J Exp Physiol Cogn Med Sci* **52**:319–330.
Southren AL, Kobayashi Y, Sherman DH, Levine L, Gordon G, and Weingold AB (1964) Diamine oxidase in human pregnancy: plasma diamine oxidase in nonpregnant and normal pregnant patients. *Am J Obstet Gynecol* **89**:199–203.
van der Linden PW, Hack CE, Poortman J, Vivié-Kipp YC, Struyvenberg A, and van der Zwan JK (1992) Insect-sting challenge in 138 patients: relation between clinical severity of anaphylaxis and mast cell activation. *J Allergy Clin Immunol* **90**:110–118.
Velicky P, Windsperger K, Petroczi K, Pils S, Reiter B, Weiss T, Vondra S, Ristl R, Dekan S, Fiala C, et al. (2018) Pregnancy-associated diamine oxidase originates from extravillous trophoblasts and is decreased in early-onset preeclampsia. *Sci Rep* **8**:6342.
Wechsler JB, Szabo A, Hsu CL, Krier-Burris RA, Schroeder HA, Wang MY, Carter RG, Velez TE, Aguiniga LM, Brown JB, et al. (2018) Histamine drives severity of innate inflammation via histamine 4 receptor in murine experimental colitis. *Mucosal Immunol* **11**:861–870.
Yamamoto M, Kiso M, Sakai-Tagawa Y, Iwatsuki-Horimoto K, Imai M, Takeda M, Kinoshita N, Ohmagari N, Gohda J, Semba K, et al. (2020) The anticoagulant nafamostat potently inhibits SARS-CoV-2 S protein-mediated fusion in a cell fusion assay system and viral infection in vitro in a cell-type-dependent manner. *Viruses* **12**:E629.
Yamaori S, Fujiyama N, Kushihara M, Funahashi T, Kimura T, Yamamoto I, Sone T, Isobe M, Ohshima T, Matsumura K, et al. (2006) Involvement of human blood arylesterases and liver microsomal carboxylesterases in nafamostat hydrolysis. *Drug Metab Pharmacokinet* **21**:147–155.

Address correspondence to: Thomas Boehm, Department of Clinical Pharmacology, Medical University of Vienna, Waehringer Guertel 18-20, 1090 Vienna, Austria. E-mail: thomas.boehm@meduniwien.ac.at